ADVANCED FUNCTIONAL MATERIALS
www.afm-journal.de

www.MaterialsViews.com

Nanoparticle Growth via Concentration Gradients Generated by Enzyme Nanopatterns

Roberto de la Rica, Erhan Bat, Karla L. Herpoldt, Hai-nan Xie, Sergio Bertazzo, Heather D. Maynard, and Molly M. Stevens**

Biomineralizing organisms can grow nanomaterials with unexpected morphologies in an organic matrix where temporal and vectorial gradients of crystal growth precursors are established. Here, concentration gradients for the crystallization of gold nanoparticles are generated and applied on silicon substrates. Gradients of crystal growth precursors are generated by enzymes patterned as lines that are separated by distances ranging from the micro- to the nanoscale. The concentration of crystallization precursors around the lines separated by nanometric distances is not only determined by mass transport and enzyme activity but also by the nanoscale organization of biocatalysts. This nanoscale organization favors non-classical crystal growth conditions that lead to the formation of nanoparticle clusters containing nanocrystals that are highly crystallographically aligned. The combination of bottom-up crystal growth with top-down electron beam lithography enables the fabrication of micrometric patterns containing gold nanoparticles of different size, shape, and surface density. These are all critical parameters that determine the physical properties of these nanomaterials.

1. Introduction

Biological crystal growth processes are an endless source of inspiration for the fabrication of materials with controlled morphologies. In biomineralization, nanoscale building blocks are often arranged with exquisite precision to generate complex shapes with a high degree of organization at the nano-, micro-, and macro-scales.[1] It has been proposed that this complex organization is made possible by non-classical crystallization pathways in which particles grow via the assembly of nanoscale building blocks.[2–4] In vitro, some key biomineralization conditions can be replicated for the generation of functional materials with controlled morphologies. For example, many biomineralization processes take place in a protein matrix in which temporal and vectorial gradients of the precursors of the reaction are established.[5] This condition can be mimicked macroscopically by using vapor diffusion of the precursors of the reaction into a liquid solution[5–7] or microscopically by controlling the rate of nucleation on substrates with micropatterned areas of different polarity.[8] While these bio-inspired approaches allow one to grow functional materials with desired shapes in mild conditions and at low cost,[5] the impact of nanoscale mass transport on the crystal growth process has not yet been systematically studied. In this context, a methodology to generate concentration gradients from nanopatterned substrates separated by well defined distances could reveal new aspects of bio-inspired crystal growth and offer a new tool for controlling the morphology of the resulting nanocrystals. Furthermore, the combination of bottom-up crystal growth with top-down lithography can offer new nanofabrication routes not available with conventional methods,[9,10] for example in the generation of highly organized nanomaterial assemblies that are difficult to fabricate with top-down methodologies alone.

In this article, we report on the spatiotemporal control of nanoparticle growth via generation of concentration gradients using nanopatterned enzymes. Enzymes are involved in biomineralization[11,12] and have been extensively used in bio-inspired approaches because they can generate crystal growth precursors in situ and act as seeding points for nucleating new crystals.[13–16] Here, we utilize the enzyme glucose oxidase (GOx) for growing gold nanoparticles as a model of crystallization of a functional material.[17–19] GOx oxidizes glucose to gluconic acid and generates hydrogen peroxide as a side product, which reduces gold ions (**Figure 1**a).[20] While this enzyme has been previously used to grow nanocrystals in nanopatterns,[17,19] the ability to control the morphology of these nanomaterials by changing the separation between GOx nanopatterns had not been studied to date, which is the key step to achieving the biomimetic crystal growth conditions in the present work. To study the effect of nanoscale organization on the growth of nanoparticles the enzymes were arranged as micrometric lines separated

Dr. R. de la Rica, K. L. Herpoldt, H.-n. Xie, S. Bertazzo, Prof. M. M. Stevens
Department of Materials
Department of Bioengineering and Institute for Biomedical Engineering
Imperial College London
Exhibition Road, London SW7 2AZ, UK
E-mail: roberto.delarica@gmail.com; m.stevens@imperial.ac.uk
Dr. E. Bat, Prof. H. D. Maynard
Department of Chemistry & Biochemistry and the California NanoSystems Institute
University of California
Los Angeles
607 Charles E. Young Drive East, Los Angeles, California 90095, USA

DOI: 10.1002/adfm.201304047

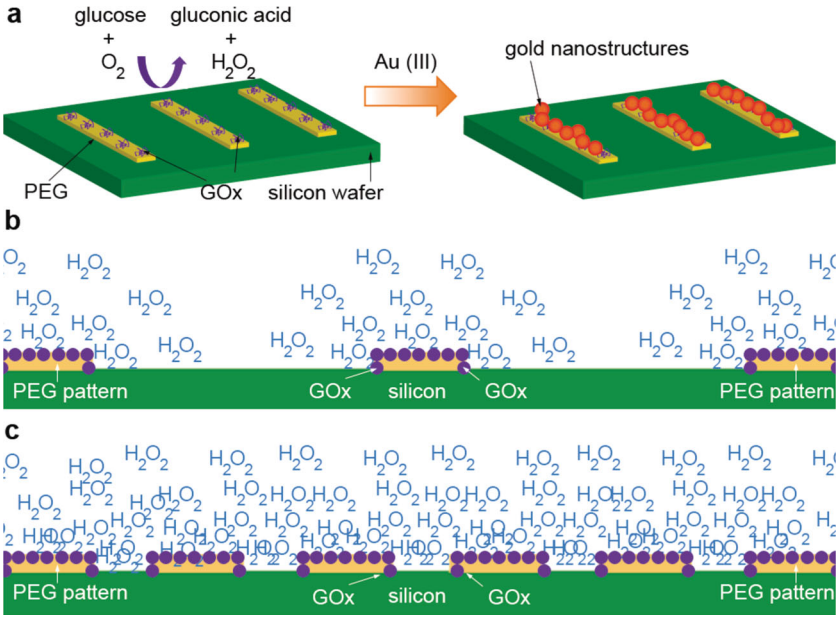

Figure 1. a) Scheme of bio-inspired growth of gold nanostructures with enzyme patterns and b,c) cross-section view schematizing the concentration profile of crystallization precursor (hydrogen peroxide) around enzyme patterns; a) reactive polyethylene glycol (PEG) patterns are covalently modified with glucose oxidase (GOx); GOx generates hydrogen peroxide in the presence of glucose, which modulates the kinetics of growth of gold nanocrystals in MES buffer; b) when the patterns are separated by micrometric distances the production of hydrogen peroxide at each pattern is independent of the production of peroxide at neighboring patterns; c) when the patterns are separated by nanometric distances the concentration profiles overlap and the nanoscale organization of enzymes plays an important role in defining the concentration of hydrogen peroxide around the patterns.

by distances ranging from 400 nm to 2 µm. In a Nernst diffusion layer, each enzyme line creates a concentration gradient of crystal growth precursor (hydrogen peroxide) from the surface of the substrate to the bulk of the solution. When the lines are separated by micrometric distances, the concentration gradient generated at each enzyme pattern is independent and not affected by neighboring patterns (Figure 1b). Under this condition the concentration of crystal growth precursor around the enzymes is solely determined by the enzyme activity and diffusion. However when the patterns are separated by nanometric distances the generation of crystal growth precursor at each pattern can influence the concentration of hydrogen peroxide in a neighboring area (Figure 1c). Therefore, the concentration of crystal growth precursors at each pattern is not only affected by the enzyme activity and diffusion of crystal growth precursors but also by the spatial organization of the enzymes at the nanoscale. It will be shown below that the nanoscale arrangement of enzymes favors non-classical crystallization pathways that result in the growth of nanoparticles with unexpected morphologies. Indeed, the correct design of enzyme patterns and reaction time can result in the growth of nanocrystals with predictable size and surface density, which are crucial nanofabrication parameters that define the physical properties of gold nanoparticles.

2. Results and Discussion

The generation of hydrogen peroxide by lines of enzymes separated by different distances was simulated in order to study the effect of the nanoscale spacings on the concentration profile of crystal growth precursors. Each enzyme was considered as a point source of hydrogen peroxide. In each line, the activity was estimated as the sum of activities of all the enzymes covering the entire surface of the pattern, in order to take the pattern size into consideration. The enzyme patterns were defined as lines of 1 µm width separated by 400 nm, 800 nm, 1 µm, and 2 µm, respectively, which are dimensions that can easily be fabricated with electron beam lithography (EBL). Mass transport was limited to diffusion in a stationary thin layer, which is a situation that can be replicated experimentally (see Section S1 in the Supporting Information). In **Figure 2**a, the concentration gradient generated by each enzyme pattern separated by 2 µm is not influenced by the production of hydrogen peroxide in a neighboring pattern. However, as the separation distance decreases below 1 µm, the concentration gradients around each pattern overlap due to the nanoscale organization of the enzymes (Figures 2b,d) and the concentration of hydrogen peroxide in the vicinity of the patterns is higher than that observed for enzyme patterns with larger separations. Therefore, simulations of mass transport around enzyme patterns indicate that the nanoscale organization can change the concentration profile of crystal growth precursors around nucleation points,

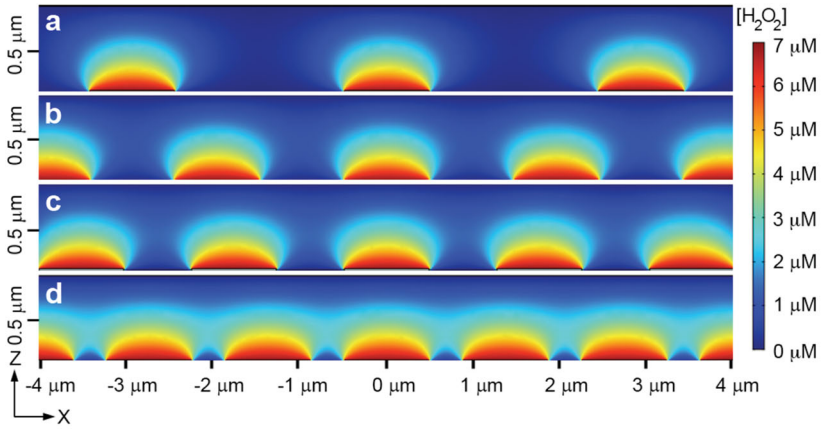

Figure 2. Cross-sectional view of a simulation showing the concentration profile of hydrogen peroxide generated by enzyme lines with a width of 1 µm and spacing between lines of: a) 2 µm; b) 1 µm; c) 800 nm, d) 400 nm.

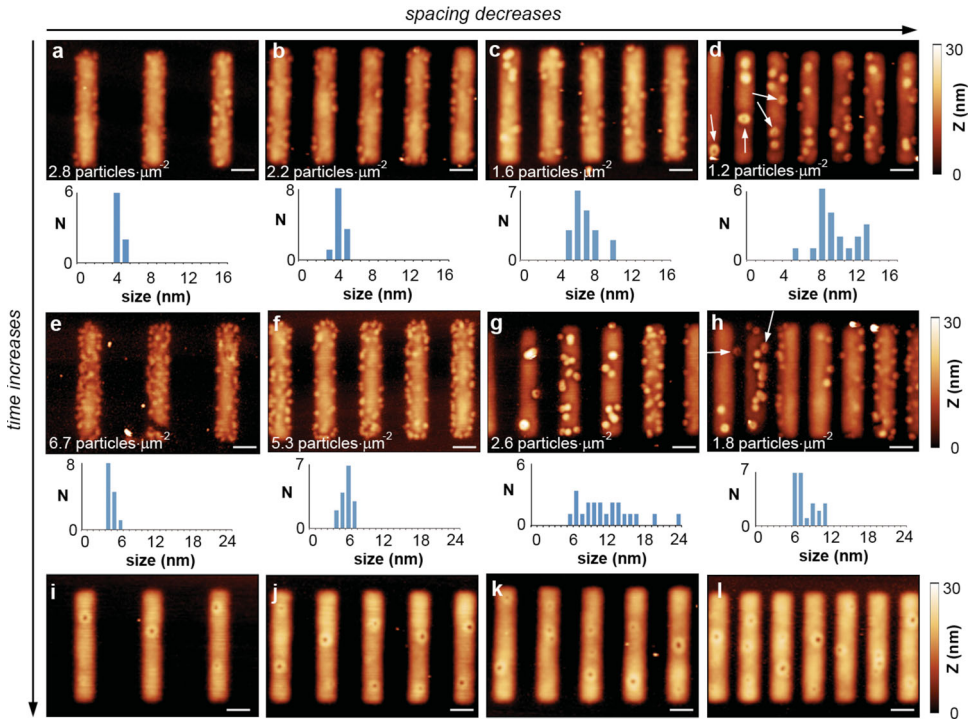

Figure 3. AFM images of enzyme patterns with different line spacing (from left to right: 2 µm, 1 µm, 800 nm and 400 nm) after triggering the growth of gold nanostructures for a–d) 5 min, e–h) 6 min, and i–l) 7 min. White arrows indicate nanoparticles with irregular shape (see also Figure S8 in the Supporting Information). Scale bars: 1 µm. Size distribution plots were obtained by measuring the height of the nanoparticles and assuming that they are spherical.

which is a key factor in defining kinetically controlled crystal growth conditions.[18]

After simulating the distribution of hydrogen peroxide around enzyme patterns, we studied the growth of gold nanoparticles with the different enzyme arrangements (Figure 1). To this end, micrometric patterns of poly(ethylene glycol) bearing carboxylic acid groups were generated on silicon substrates by electron beam lithography.[21–23] Subsequently, glucose oxidase was covalently immobilized on the polymer pads via amide bond formation without noticeable loss in activity (Sections S2–4 of the Supporting Information). The substrates were then immersed in a stirred solution containing MES buffer so that the enzyme patterns were perpendicular to the agitation vortex (Section S1 of the Supporting Information). Under this condition a stationary thin layer is formed in which mass transport is governed by diffusion.[24] The substrates were immersed in a relatively large volume to ensure that concentration gradients were not affected by changes in the properties of the bulk of the solution. Glucose was added at a concentration high enough to saturate the enzymes. Gold (III) chloride was added 10 seconds after triggering the biocatalytic production of hydrogen peroxide. After different reaction times, the substrates were rinsed with water and dried with nitrogen and their topography was studied with atomic force microscopy (AFM). **Figure 3** summarizes the main results obtained with different enzyme arrangements after 5 min (Figures 3a–d), 6 min (Figures 3e–h) and 7 min (Figures 3i–l) reaction time. It is apparent that gold nanoparticles were grown after 5 and 6 min reaction time whereas a smooth gold coating was obtained after 7 min. The growth of gold nanoparticles on the substrates was validated by the observation of surface enhanced Raman scattering (SERS) signals typical of gold nanostructures (Figure S5 in the Supporting Information). Furthermore, the same experiments performed with inactivated enzymes yielded only a few nanoparticles and very low SERS signals, therefore demonstrating that the enzyme activity is a key factor for growing gold nanostructures (Figures S6,S7 in the Supporting Information). To show the relevance of the enzyme-generated concentration gradients of crystal growth precursors in controlling the morphology of nanoparticles, we repeated the same experiments with substrates containing inactivated enzymes but adding 7 µM H_2O_2 to the solution. This concentration value was obtained from simulations in Figure 2 (≈7 µM at the surface of the pattern). Under this condition, gold coatings, but not discrete nanoparticles, were observed on the enzyme patterns (**Figure 4**). As expected from gold reduction in the absence of concentration gradients, the thickness of the gold coating increases as the time increases. These experiments demonstrate that generating gradients of crystal growth precursors with enzymes is the key step to generating nanomaterials of different morphology (nanoparticle vs coating and nanoparticles of different size) under the proposed conditions.

When crystal growth is governed by active enzyme patterns separated by 2 µm, small nanocrystals with a diameter of ca. 4 nm are observed on the patterns after 5 and 6 min (Figures 3a and 3e, respectively). After 7 min, the nanoparticles coalesce to form a smooth coating on the surface (Figure 4i and Figure S7 in the Supporting Information). These results indicate that, when

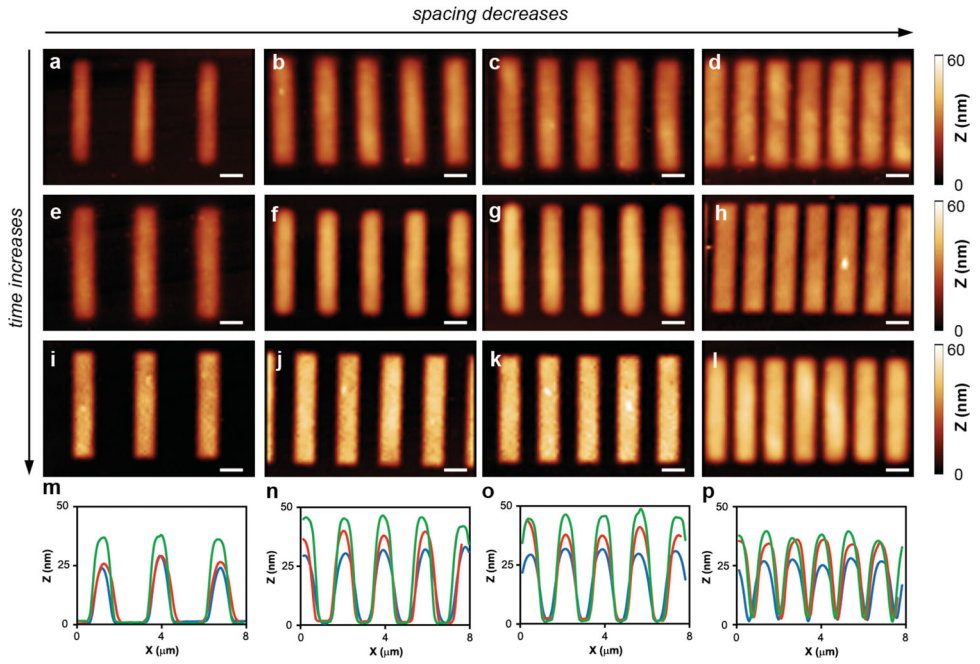

Figure 4. AFM images of inactive enzyme patterns with different line spacings (from left to right: 2 μm, 1 μm, 800 nm and 400 nm) after triggering the reduction of gold nanostructures with 10 μM hydrogen peroxide for a–d) 5 min, e–h) 6 min, and i–l) 7 min. Scale bars: 1 μm. Cross-sectional height plots showing the average height of enzyme patters after 5 min (blue), 6 min (red), or 7 min (green) calculated from AFM images in which the enzyme lines are separated by: m) 2 μm; n) 1 μm; o) 800 nm, and p) 400 nm.

the patterns are separated by micrometric distances, increasing the reaction time favors the nucleation of new nanocrystals on the enzyme patterns rather than the growth of larger nanoparticles. Similarly, when the enzyme lines are separated by 1 μm the number of nanocrystals increases with time until a smooth coating is generated (Figures 3b,f,j). A slight increase in the size of the nanocrystals is observed after 6 min compared to the 5 min situation. More distinct variations are observed upon entering the nanoscale regime. When the patterns are separated by 800 nm, larger nanoparticles are found after 5 min (Figure 3c). Even larger nanoparticles of different sizes are observed after 6 min (Figure 3g), and the smooth coating is obtained after 7 min (Figure 3k). The surface density of nanoparticles also decreases noticeably. A similar trend is observed for enzyme patterns separated by 400 nm: the nanoparticles are large, show a polydisperse size distribution and are less abundant than in the case of enzyme lines separated by micrometric distances (Figures 3d,h). Summarizing, the results shown in Figure 3 suggest that a longer reaction time favors the nucleation of new nanoparticles. After 6 min, the nanoparticles are so abundant that they coalesce and form a coating on the surface, as demonstrated by SERS spectroscopy (Figure S7 in the Supplementary Information), and patchy, rough coatings between 6 and 7 min after triggering the reduction of gold were observed (Figure S8 in the Supplementary Information). Since such a coating blocks the production of crystal growth precursors by the enzyme, the nanoscale architecture is not relevant in defining changes under this condition, which explains the similar results obtained in Figures 3i–l. Regarding the spatial organization of concentration gradients, reducing the line spacing to the nanoscale favors the growth of larger and less abundant nanoparticles (see Figure S9 in the Supporting Information). All in all, the results shown in Figure 3 demonstrate that parameters such as surface density, nanoparticle size, and shape (nanoparticle vs coating) can be manipulated by the reaction time and concentration gradients defined by the nanoscale organization. Indeed, for nanoscale spacings, there is a linear relationship between the pattern spacing and the size of the nanoparticles for a growth time of 5 min (Section S9 in the Supporting Information). This "scaling law" could be useful for the utilization of enzyme patterns in the bottom-up nanofabrication of gold nanoparticles with predetermined size and surface density.

The outcome in Figure 3 that nanoscale separation of enzyme patterns favors the growth of larger nanoparticles is intriguing from a classical crystallization point of view. It was shown in Figure 2 that the concentration of crystal growth precursors around the enzyme patterns is larger for patterns separated by nanoscale distances. Usually, increasing the concentration of hydrogen peroxide leads to faster kinetics of growth,[8] which in turn favors the nucleation of new nanoparticles. If nucleation is favored, smaller and more abundant nanoparticles should be obtained when the patterns are separated by nanometric spacings. This is in contrast with our results in Figure 3 in which larger and less abundant nanoparticles are found with nanopatterns. Furthermore, we observed that several nanoparticles show irregular surfaces (white arrows in Figures 3d,h, see also Figure S10 in the Supplementary Information). To clarify this point, we performed solution-based experiments to study changes in the morphology of the nanoparticles with variations of peroxide concentration around the maximum value in Figure 2 (7 μM). **Figure 5**a shows UV-Vis spectra of nanoparticle solutions 6 min after adding hydrogen peroxide

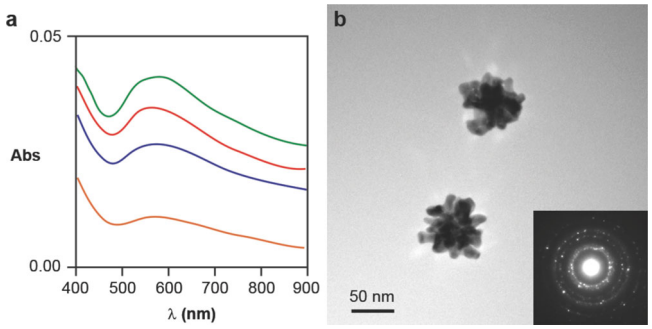

Figure 5. Growth of gold nanoparticles in solution; a) UV-Vis spectra of nanoparticle solutions 6 min after adding hydrogen peroxide with the concentration of 0 μM (orange), 1 μM (blue), 3 μM (red), and 10 μM (green); b) TEM images of gold nanoparticles grown with 10 μM hydrogen peroxide. Inset: SAED pattern of a group of particles.

with the concentration of 0, 1, 3, and 10 μM. Nanoparticles can grow slowly in the absence of hydrogen peroxide because 2-(N-morpholino)ethanesulfonic acid (MES) and glucose act as weak reducing agents.[25] It is evident from the UV-Vis spectra that the addition of hydrogen peroxide accelerates the kinetics of growth. In these spectra, the position of the localized surface plasmon resonance (LSPR) shifts from 555 to 565, 566, and 574 nm, when the concentration of hydrogen peroxide increases from 0 to 1, 3, and 10 μM, respectively. The observed red-shift when increasing the concentration of hydrogen peroxide is in accordance with the growth of larger or more aggregated nanoparticles.[26] These results are in agreement with the observation in Figure 2 and Figure 3 that a shorter distance between patterns leads to the formation of larger nanoparticles due to the presence of higher levels of hydrogen peroxide. It should be noted that decreasing the levels of glucose by a much larger concentration (1 mM) does not have any effect in the LSPR of the nanoparticles, therefore demonstrating that the consumption of glucose by the enzyme does not play an important role in nanoparticle growth (Section S12 in the Supporting Information). Transmission electron microscopy (TEM) images show irregular nanoparticles that are formed via aggregation of smaller nanocrystals (Figure 5b). The observation of the d-spacings of the planes (111), (022), and (113) with selected area electron diffraction (SAED) demonstrate the growth of crystalline gold (Figure 5b, inset).

The visualization of clusters containing aggregated nanocrystals in Figure 5b suggests that the nanoparticles do not grow via classical pathways. Two alternative routes could explain the results seen in Figure 5. On the one hand, it has been reported that gold nanoparticles may have GOx-mimicking properties that result in the self-catalyzed, self-limiting growth of gold nanoparticles on gold seeds.[27] Under this condition, gold seeds generate hydrogen peroxide and this results in the growth of gold nanoparticle satellites around them, which then grow to generate clusters of gold nanoparticles. On the other hand, the growth of nanoparticle clusters could be the result of non-classical crystal growth conditions in which the assembly of nanoscale building blocks is used as an efficient way to reduce the surface energy of the growing nanocrystals, as previously observed in biomineralization processes.[2–4] In this non-classical crystal growth route, the constituent nanocrystals are often aligned with exquisite accuracy. To elucidate the main mechanism of nanoparticle growth, we studied the morphology of the nanoparticles at different stages of the growth process with TEM. **Figure 6** shows representative TEM images of the nanoparticles obtained 4, 5, 6, and 7 min after triggering the reduction of gold. In these images, smaller nanoparticles supported on gold seeds were not seen even at the early stages of crystal growth. Furthermore, it was found that the gold nanoparticles did not have GOx-mimicking properties, that is, they could not generate noticeable levels of hydrogen peroxide under the proposed conditions (Section S11 in the Supporting Information). These experiments confirmed that the nanoparticle clusters do not grow by means of self-catalyzed, self-limiting routes but via non-classical crystal growth conditions that imply the aggregation of nanoparticle building blocks. This was further sustained by the observation in Figure 6e that the lattice fringe of the plane (002) crosses different nanoparticles (areas of different electron density) with little or no misalignment.[28] Furthermore the SAED of the whole cluster shown in the inset of Figure 6e resembles the SAED of a single crystal, as expected from nanocrystals that are highly crystallographically aligned.[28] This "oriented attachment" of nanoparticle building blocks is often found in biomineralization[2] and bio-inspired crystal growth,[28] and therefore it strongly supports the hypothesis that the nanoparticles grow via non-classical crystal growth pathways.

In the context of biomimetic crystal growth, the results in Figure 3 can be interpreted as follows. When the patterns are separated by micrometric distances the concentration of hydrogen peroxide around the pattern is low (Figures 2a,b). These slow growth conditions favor the nucleation of nanocrystals on the enzyme patterns as seeding points, which results in smaller, more abundant nanoparticles. However, when the patterns are separated by nanometric distances the concentration of

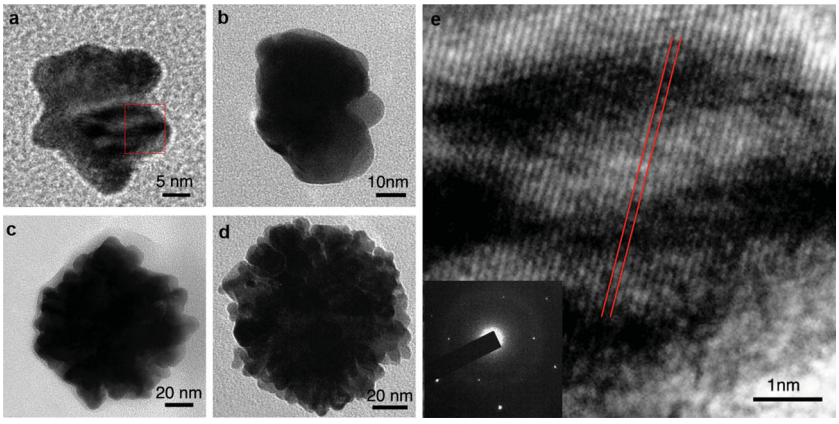

Figure 6. TEM images of gold nanoparticles grown with 10 μM hydrogen peroxide after: a) 4 min; b) 5 min; c) 6 min; d) 7 min; e) enlarged image of the area inside the red square in (a) showing the lattice fringe of the plane (002) crossing areas of different electron density without misalignment (highlighted in red); SAED of the cluster in (a).

hydrogen peroxide around the patterns is higher (Figure 2c,d). Under this condition the nanoparticles nucleate fast in solution and aggregate in order to reduce their surface energy. Therefore, although nucleation is favored at higher peroxide concentrations, the resulting nanoparticles are larger and less abundant because they are formed by the assembly of several nanoscale building blocks. This growth by aggregation of nanometric building blocks also explains the observation of irregular topographies in the nanoparticles grown with nanoscale patterns (white arrows in Figure 3d,h and Figure S8 in the Supporting Information).

3. Conclusions

In conclusion, the effect of spatial organization at the nanoscale on enzyme-guided crystal growth was studied. When patterned on a substrate, the enzymes generate concentration gradients of crystal growth precursors. The nanoscale organization of patterns favors non-classical growth conditions in which nanoparticles grow via assembly of nanoscale building blocks rather than by incorporation of atoms to existing nuclei. This phenomenon results in the formation of large clusters of nanocrystals when the distance between enzyme patterns is reduced below 1 μm. Increasing the reaction time leads to an increase in the number of nanoparticles on the surface first, and then to a change in the overall morphology from discrete nanocrystals to smooth coating. The ability to control the size, surface density and state of aggregation of the nanocrystals could be of great impact in tuning the optical properties of the nanoparticles, for example, in SERS imaging and biosensing applications.[26,29] Since nanoparticle growth is based on the local generation of concentration gradients, nanoparticles with different morphologies could be grown simultaneously on the wafer by patterning different areas with lines separated by predetermined distances. Furthermore, we envisage that the methodology could be adapted for the fabrication of other functional materials such as titanium dioxide,[30] gallium oxide,[31] or silver sulfide,[32] whose growth can be triggered by enzymes. Moreover, the resulting micrometric patterns containing nanostructured functional materials could potentially be integrated with microfabricated circuit elements as a crucial step in the fabrication of next-generation biosensors and microprocessors.[10]

4. Experimental Section

Preparation of PEG-COOH Patterned Substrates:[21–23] Si chips were cleaned by immersing in freshly prepared piranha solution (3:1 H_2SO_4/H_2O_2, Caution! Piranha solution reacts violently with organic materials.). The chips were then washed with a copious amount of MilliQ water and dried under a stream of air. Cleaned Si chips were spin-coated (2000 rpm for 20 s, 4000 rpm for 10 s) with 2 wt% 8-arm PEG-COOH (JenKem Technology U.S.A., MW = 20000 g mol^{-1}) solution in 1,2-dichloroethane. The coated chips were then used directly without any drying or baking steps. Pattern files for electron beam lithography were created using DesignCAD Express 16 software. Arrays of rectangular (1 μm × 5 μm) polymer patterns comprising a range of spacings in between (400, 800, 1000, 2000 nm) were generated using a JC Nabity e-beam lithographic system (Nanometer Pattern Generation System, version 9.0) modified from a JEOL JSM-6610 scanning electron microscope. An accelerating voltage of 30 kV was used, with a beam current of ≈15 pA, a spot size of 32 nm, and using an area dose of 30 μC cm^{-2}. After e-beam exposure, any non-crosslinked polymer on the chips was rinsed with methanol, water, and methanol (10 s each) and the substrates were dried with a stream of nitrogen. Pattern formation was confirmed using an inverted bright-field microscope. The height of the patterns was 15 to 50 nm as determined by atomic force microscopy.

Immobilization of Glucose Oxidase on PEG-COOH Patterned Surfaces:[33] The prepared surfaces were activated using 0.1 M 1-ethyl-3-(3-dimethylaminopropyl)carbodiimide (EDC, Sigma-Aldrich) and 0.2 M N-hydroxysuccinimide (NHS, Sigma Aldrich) in 0.1 M 2-(N-morpholino) ethanesulfonic acid buffer (MES buffer, pH 5.5) for 1 h. After rinsing with MES buffer, the substrates were immediately incubated with 1 mg mL^{-1} of glucose oxidase from Aspergillus Niger (GOx, Sigma-Aldrich) solution in phosphate buffered saline (PBS, pH 7.4). Then, the surfaces were washed with 0.1% (v/v) Tween 20 in PBS, rinsed with water and dried with nitrogen. Inactive enzyme patterns were obtained by heating the GOx-modified substrates at 70 °C for 30 min.

Simulations: Simulations were made assuming the generation of a Nernst diffusion layer close to the PEG patterns (see Section S1 in the Supporting Information). Within this region mass transport can be considered to be diffusion-limited and convection effects negligible. Simulations were solved using Finite Element Analysis (FEA) in COMSOL Multiphysics.

Fick's law was solved in the steady state under the above assumptions. The flux of hydrogen peroxide molecules generated at the surface was calculated using:

$$\varphi = \frac{\nu}{D2\pi r} \quad (1)$$

where ν is the specific activity of the enzyme, 0.44 × 10^{-21} mols s^{-1} $molecules^{-1}$ (value provided by the manufacturer) and D is the diffusion coefficient for hydrogen peroxide, 1.5 × 10^{-9} m^2 s^{-1}.[34] GOx has a diameter of ≈7 nm as measured by dynamic light scattering (DLS).[35] The surface density of enzymes (150 enzymes/pattern) was estimated assuming spherical particles forming a compact monolayer on PEG patterns (see Section S3 in the Supporting Information). Close to the surface (r = 7 nm) the initial concentration of hydrogen peroxide is thus calculated using Equation () to be 7 × 10^{-6} M. The concentration of hydrogen peroxide in the bulk solution is initially assumed to be 0. Spacings between PEG pads were varied to match the experimental design.

Growth of Gold Nanoparticles: 1 mM MES buffer was prepared by diluting a 0.1 M MES buffer solution (pH 6). Substrates containing enzyme patterns were immersed in a 100 mL beaker containing 90 mL of 1 mM MES stirred with a magnetic stirrer (900 rpm) (see Section S1 in the Supporting Information). The production of hydrogen peroxide was triggered via the addition of 10 mL of 1 M glucose in 1 mM MES. After 10 s, 100 μL of a 100 mM gold (III) chloride trihydrate solution was added to the stirring solution. After 5, 6, or 7 min, the substrates were rinsed with water and dried with nitrogen. AFM images were taken in tapping mode with a Veeco Multimode instrument. Images were processed with Gwyddion. Solution based experiments were performed in exactly the same way but adding hydrogen peroxide to the final desired concentration prior to the addition of gold chloride. After 6 min, a 1 μL drop was placed on a carbon grid and dried with a piece of filter paper. The remaining nanoparticles were imaged with a JEOL 2000FX TEM working at an acceleration voltage of 200 kV (Figure 5b) or with a Jeol 2100F TEM working at an acceleration voltage of 80 kV (Figure 6). UV-Vis spectra were obtained with a Lambda 25 spectrometer (Perkin Elmer).

Supporting Information

Supporting Information is available from the Wiley Online Library or from the author.

Acknowledgements

R. de la R. and E.B. contributed equally to this work. This research was supported by a Marie Curie Intra European Fellowship within the 7th European Community Framework Programme (R.d.l.R.). E.B. thanks The Netherlands Organization for Scientific Research and Marie Curie Cofund Action for the financial support (Rubicon Grant 680–50–1101). M.M.S. thanks EPSRC grant EP/K020641/1 and the Leverhulme Trust (VP2–2011–016) for funding. H.D.M. thanks the National Science Foundation through SINAM (DMI-0327077) and the Burroughs Wellcome Fund for funding. S.B. was supported by the Junior Research Fellowship scheme at Imperial College London.

Received: December 2, 2013
Revised: January 14, 2014
Published online: February 26, 2014

[1] J. Aizenberg, J. C. Weaver, M. S. Thanawala, V. C. Sundar, D. E. Morse, P. Fratzl, *Science* **2005**, *309*, 275–278.
[2] M. Niederberger, H. Coelfen, *Phys. Chem. Chem. Phys.* **2006**, *8*, 3271–3287.
[3] W. J. E. M. Habraken, J. Tao, L. J. Brylka, H. Friedrich, L. Bertinetti, A. S. Schenk, A. Verch, V. Dmitrovic, P. H. H. Bomans, P. M. Frederik, J. Laven, P. van der Schoot, B. Aichmayer, G. de With, J. J. DeYoreo, N. A. J. M. Sommerdijk, *Nat. Commun.* **2013**, *4*, 1507.
[4] J. Fang, B. Dinga, H. Gleiter, *Chem. Soc. Rev.* **2011**, *40*, 5347–5360.
[5] R. L. Brutchey, D. E. Morse, *Chem. Rev.* **2008**, *108*, 4915–4934.
[6] T. Ould-Ely, M. Luger, L. Kaplan-Reinig, K. Niesz, M. Doherty, D. E. Morse, *Nat. Protoc.* **2011**, *6*, 97–104.
[7] D. Kisailus, B. Schwenzer, J. Gomm, J. C. Weaver, D. E. Morse, *J. Am. Chem. Soc.* **2006**, *128*, 10276–10280.
[8] J. Aizenberg, A. J. Black, G. M. Whitesides, *Nature* **1999**, *398*, 495–498.
[9] N. Nuraje, S. Mohammed, L. L. Yang, H. Matsui, *Angew. Chem. Int. Ed.* **2009**, *48*, 2546–2548.
[10] R. de la Rica, K. I. Fabijanic, A. Baldi, H. Matsui, *Angew. Chem. Int. Ed.* **2010**, *49*, 1447–1450.
[11] A. Schulz, H. Wang, P. van Rijn, A. Böker, *J. Mater. Chem.* **2011**, *21*, 18903–18918.
[12] M. A. Rahman, T. Oomori, T. Uehara, *Mar. Biotechnol.* **2007**, *10*, 31–38.
[13] R. de la Rica, H. Matsui, *Angew. Chem. Int. Ed.* **2008**, *47*, 5415–5417.
[14] M. Wiens, T. Link, T. A. Elkhooly, S. Isbert, W. E. G. Muller, *Chem. Commun.* **2012**, *48*, 11331–11333.
[15] I. Sondi, S. D. Skapin, B. Salopek-Sondi, *Cryst. Growth Des.* **2008**, *8*, 435–441.
[16] K. I. Fabijanic, R. Perez-Castillejos, H. Matsui, *J. Mater. Chem.* **2011**, *21*, 16877–16879.
[17] B. Basnar, Y. Weizmann, Z. Cheglakov, I. Willner, *Adv. Mater.* **2006**, *18*, 713–718.
[18] L. Rodriguez-Lorenzo, R. de la Rica, R. A. Alvarez-Puebla, L. M. Liz-Marzan, M. M. Stevens, *Nat. Mater.* **2012**, *11*, 604–607.
[19] M. Zayats, R. Baron, I. Popov, I. Willner, *Nano Lett.* **2005**, *5*, 21–25.
[20] R. de la Rica, M. M. Stevens, *Nat. Nanotechnol.* **2012**, *7*, 821–824.
[21] K. L. Christman, E. Schopf, R. M. Broyer, R. C. Li, Y. Chen, H. D. Maynard, *J. Am. Chem. Soc.* **2009**, *131*, 521–527.
[22] Y. Hong, P. Krsko, M. Libera*Langmuir* **2004**, *20*, 11123–11126.
[23] C. M. Kolodziej, H. D. Maynard, *Chem. Mater.* **2012**, *24*, 774–780.
[24] R. de la Rica, A. Baldi, C. Fernández-Sánchez, *Appl. Phys. Lett.* **2007**, *90*, 074102 .
[25] C. Engelbrekt, K. H. Sorensen, J. D. Zhang, A. C. Welinder, P. S. Jensen, J. Ulstrup, *J. Mater. Chem.* **2009**, *19*, 7839–7847.
[26] N. Pazos-Perez, C. S. Wagner, J. M. Romo-Herrera, L. M. Liz-Marzan, F. J. G. de Abajo, A. Wittemann, A. Fery, R. A. Alvarez-Puebla, *Angew. Chem. Int. Ed.* **2012**, *51*, 12688–12693.
[27] W. Luo, C. Zhu, S. Su, D. Li, Y. He, Q. Huang, C. Fan, *ACS Nano* **2010**, *4*, 7451–7458.
[28] J. Fang, S. Du, S. Lebedkin, Z. Li, R. Kruk, M. Kappes, H. Hahn, *Nano Lett.* **2010**, *10*, 5006–5013.
[29] J. Xie, Q. Zhang, J. Y. Lee, D. I. C. Wang, *ACS Nano* **2008**, *2*, 2473–2480.
[30] L. A. Bawazer, M. Izumi, D. Kolodin, J. R. Neilson, B. Schwenzer, D. E. Morse, *Proc. Natl. Acad. Sci. U.S.A.* **2012**, *109*, E1705–E1714.
[31] D. Kisailus, J. H. Choi, J. C. Weaver, W. J. Yang, D. E. Morse, *Adv. Mater.* **2005**, *17*, 314–318.
[32] C. Pejoux, R. de la Rica, H. Matsui, *Small* **2010**, *6*, 999–1002.
[33] N. Nakajima, Y. Ikada, *Bioconjugate Chem.* **1995**, *6*, 123–130.
[34] S. A. M. van Stroe-Biezen, F. M. Everaerts, L. J. J. Janssen, R. A. Tacken, *Anal. Chim. Acta.* **1993**, *273*, 553–560.
[35] I. Otsuka, M. Yaoita, S. Nagashima, M. Higano, *Electrochim. Acta* **2005**, *50*, 4861–4867.